SIMULATION OF CHANGES IN TEMPERATURE AND PRESSURE FIELDS DURING HIGH SPEED PROJECTILES FORMING BY EXPLOSION

by

Miloš D. MARKOVIĆ[a*], Momčilo P. MILINOVIĆ[a], Olivera M. JEREMIĆ[a], and Slobodan S. JARAMAZ[a]

[a] Faculty of Mechanical Engineering, University of Belgrade, Belgrade, Serbia

Original scientific paper
DOI:10.2298/TSCI151217073M

The research in this paper considered the temperatures fields as the consequently influenced effects appeared by plastic deformation, in the explosively forming process aimed to design explosively formed projectiles. As the special payloads of the missiles, used projectiles are packaged as the metal liners, joined with explosive charges, to design explosive propulsion effect. Their final form and velocity during shaping depend on distributed temperatures in explosively driven plastic deformation process. Developed simulation model consider forming process without metal cover of explosive charge, in aim to discover liner's dynamical correlations of effective plastic strains and temperatures in the unconstrained detonation environment made by payload construction. The temperature fields of the liner's copper material are considered in time, as the consequence of strain/stress displacements driven by explosion environmental thermodynamically fields of pressures and temperatures. Achieved final velocities and mass loses as the expected explosively formed projectiles performances are estimated regarding their dynamical shaping and thermal gradients behavior vs. effective plastic strains. Performances and parameters are presented vs. process time, numerically simulated by the Autodyne software package.

Key words: *explosively formed projectiles, explosive propulsion, temperature and pressure profiles, effective plastic strain, numerical simulation*

Introduction

Advance concept design of high-speed projectiles, by using directed mechanical energy of explosion is known as the explosively formed projectiles (EFP) [1-4]. Most frequently, these designing concepts are used to penetrate targets from the appropriated distances [1-3, 5, 6]. Used sub-projectiles are packaged as the metal liners, joining with explosive charges, to design explosive propulsion effect. The papers [3, 7, 8] supposed applications with additional gimbaled mechanism for the payloads of antiballistic guided missiles.

Initial high velocity of EFP is the complex function of several processes and parameters integrated into the warheads' subassemblies. By explosion effect [9, 10], metal liner [1, 2, 11-13], integrated with explosive charge, takes the part of explosive detonation energy [6, 14, 15] reshapes its initial form, and transforms it into the kinetic energy of EFP. The performances, of the EFP are cause-co sequencing relationship of the temperature and deformation of metal liner appeared in, dynamically, observed testing conditions. Particular temperatures distribution

* Corresponding author; e-mail: mdmarkovic@mas.bg.ac.rs

along liner in the forming process, is subject considered in this paper, and is presented by the copper metal liner capable to form in to the projectile driven by explosive propulsion.

The problem of temperature and its influence on the liner's deformation is presented in the papers [1, 16-18]. The numerical approach in the papers [17, 19, 20] is set up to test the influencing comparative parameters of the temperature values and initial velocity of the EFP as its dynamical performance. In the paper [1] the basic statement about shaping of EFP is exposed as the condition that effective plastic strain has to be constant in shaping time, to avoid liner mass loses, made by critical stretching during prompt deformation. Copper, as the liner material during EFP forming, showed good experimental data fitting by the Johnson-Cook and Zerilli–Armstrong strain-stress equations. Model provided by author to estimates deformation vs. relative temperatures exposed by the thermal softening term in Johnson-Cook equation [16]. Regardless authors explained very precise behavior of experimentally finished EFP samples, they did not observed behavior of temperatures and strains for the particular liner's segments.

Paper [17], as well as [1] seem more comprehensive regarding average values of temperatures and deformation energy vs. time but also missed particular considerations of mentioned performances along liner. Deformation analyses derived by [14] used Johnson-Cooks' approximation for the strain-stress and absorbed energy, valid for the process of plastic deformation as the cause for the increasing temperatures in the roughly observed parts of liners' volume.

In the cited papers, only the average temperature of the liner is considered, and the temperatures of local elements of liners' deformable body are missing. In addition, noted cited papers lack derivation of the temperature-time profiles of the critical elements observed in liners, important for the avoiding of local deformation discontinuity, able to make liners' parts fracture and, consequently, mass loses during forming of final EFP velocity. This is approved by the authors [1], who stated that gradient of deformation in any point of liner has to be more or less constant in time.

These analyses proved orientation of this paper on more precise research of the local and comprehensive analyses of deformation temperature, in the appropriated number points on liner *vs*. process's time to be realized in the numerical tests.

Temperature and gas-dynamical field behind and in front of projectile are also very complex and dependable of the EFP shape, which changes in time, and consequently changes the flight drag coefficients. Except notes in the papers [2, 18], this area is not well covered by the available literature. In that, sense, research in this paper, is the contribution to this topic, made by the researched simulation.

Simulation sample

The testing sample in this paper is the EFP copper liner joint with fixed cylindrical frame explosive charge designed without metal cover. Developed simulation model has considered effect without metal cover of explosive charge, to discover liner's dynamical correlations of effective plastic strain and temperature correlations, made only by lateral unconstrained explosion without collateral cover influences. In that sense, the simulation sample does not include additional components usually integrated in to the warheads' assembly. Dimensions and design characteristics of the testing sample are shown in fig. 1. The properties of explosive and liner material used in simulations are shown in tabs. 1 and 2. The initiation point of explosion is at the bottom of the sample charge in fig. 1. All required data about materials are within menu offered by software package Autodyne [21] and given in tab. 2.

Numerical method

Numerical approach with adopted simulation grid [20-25] valid for the Euler model is used for the EFP obtained velocity and temperature distribution, as well as, for estimations of the projectile shape. The 2-D semi cross-section of explosive charge with liner shaping control volume used in numerical simulation has shown in fig. 2.

Two groups of points are presented. First one, number 1-30, for the expected movable parts of liner during EFP forming process, and second, with fixed points, number 31-54, to control distributions of forming process during explosion along control distance of central line. Also, boundary conditions shown around observed area, are of "flow out" type to avoid effects of detonation reflections during propagation process. In that sense of detonation, products (henceforth DP) have free expansion out of this boundary. The density of the numerical grid has been determined by the 2000×200 elements along x-y directions according to accuracy as well as reasonable simulation run time within available computer facilities.

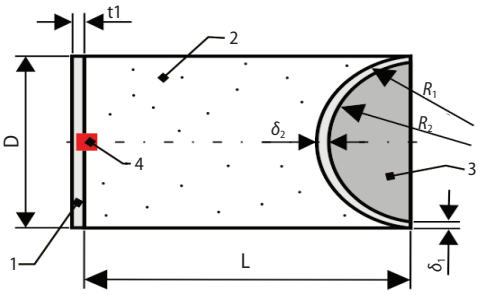

Figure 1. Basic dimensions of testing sample; *1 – back plate, 2 – explosive charge (OCTOL), 3 – liner (copper), 4 – initiation point*

Table 1. Geometrical parameters for EFP testing assembly

Design parameter		
Length of charge	L [mm]	200
Caliber (diameter)	D [mm]	150
Liner thickness	$\delta_1 = \delta_2$ [mm]	10
Type of initiation	point initiation	
Radii	R_1=R_2 [mm]	150

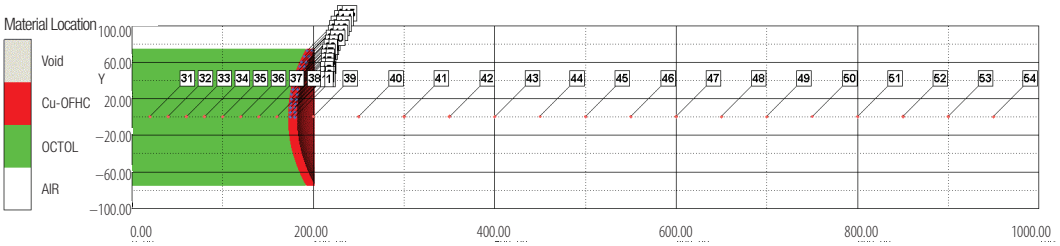

Figure 2. Fixed control points and boundaries of the considered area of simulation (*for color image see journal web site*)

Pressure of detonation products DP is determined in the Autodyne software package according to Jones-Wilkins-Lee, (henceforth JWL), equation of state [1, 2] in the form:

$$p = A_1\left(1-\frac{\omega}{R_1V}\right)\mathrm{e}^{-R_1V} + B_1\left(1-\frac{\omega}{R_2V}\right)\mathrm{e}^{-R_2V} + \frac{\omega E}{V} \tag{1}$$

where each coefficient for appropriate explosive [1, 2] is given in tab. 2.

Detonation and detonation products (henceforth DP) temperatures are determined with the BKW equation of state [1, 26, 27] given in the form:

$$\frac{pv_g}{\mathrm{R}T} = 1 + Xe^{\beta X}, \quad X = \frac{\chi\sum_i x_i k_i}{v_g(T+\theta)^{\alpha}} \tag{2}$$

Table 2. Input parameters from Autodyne for numerical simulation

JWL parameters for OCTOL			Cu-OFHC (copper) parameters			Air parameters		
	Values	Units		Values	Units		Values	Units
A	$7.486\cdot10^8$	kPa	Density	8.96	g/cm^3	ρ_{AIR}	1.225	kg/m^3
B	$1.338\cdot10^7$	kPa	Bulk modulus	$1.29\cdot10^8$	kPa	γ	1.4	–
R_1	4.5	-	Ref. temperature	300	K	T_0	288.2	K
R_2	1.2	-	Specific heat	383	J/kgK	c_p	717.6	kJ/kgK
ω	0.38	-	Johnson Cook parameters for Cu-OFHC					
ρ_0	1.821	g/cm^3	Shear modulus	$4.6\cdot10^7$	kPa			
CJ detonation state for JWL products EOS for OCTOL			A_1	$9\cdot10^4$	kPa			
			B_1	$2.92\cdot10^5$	kPa			
D	$8.48\cdot10^3$	m/s	n	0.31	–			
P	$3.42\cdot10^7$	kPa	C	0.025	–			
E	$9.6\cdot10^6$	kJ/m^3	m	1.09	–			
			T_m	$1.365\cdot10^3$	K			
			$\dot{\varepsilon}$	1	–			

This general BKW-EOS (equation of state) is also stated in literature [26], but with different noted coefficient X as K. Paper [27] noted that among all BKW-EOS as it, BKWR, BKWC, BKWS, which are variations of the BKW, but with different fitting constants, the most comprehensive and precise is the BKWS-EOS. The referencing temperature from eq. 2 based on BKWS fitted constants, for explosive material OCTOL [27], is also taken in this research. Liner temperatures as well as the deformation temperature of liner shaping process which transforms into the EFP are calculated by the relations of effective plastic strain and stresses initiated by the mechanical energy of detonation products by the Johnson- Cook equation [2, 16] in the form:

$$\sigma = (A + B\varepsilon^n)(1 + C\log\dot{\varepsilon}^*)(1 - T_H^m) \tag{3}$$

where each value for the coefficients for appropriate liner material is given in tab. 2 according to [1, 2].

Simulation results and data analysis

EFP external loadings simulation

Dynamical performances and results of EFP forming process in the high-speed projectile from the liner propelled by the distributed detonation pressure (DP), during and after explosion are on fig. 3. To observe liners behavior during process a liner cross section is divided into two areas, with 30 observed points. First 15 points is on back liners' layer (henceforth - back layer) which is in the contact with the explosive, and second 15 points are on the front liners' layer (henceforth front layer) which is in the direction of motion and shown on fig. 5. Back surface, which contain observed dynamical points number 16-30 (fig. 5), are in contact with explosive charge, at the very beginning, fig. 3(a), EXP, and with detonation products DP during process of time sequences. Process propagates figs. 3(a), 3(b), 3(c), 3(d), and fig. 3(e) in time sequences with increasing velocity (dashed arrow fig. 3), after initiation at the instant $t = 0$ μs along axial direction x, over fixed noted points number 39-54 (fig. 2). Both, back and front layers are the parts of one, full surface of the liner, but with different plastic tensile *vs*. time in the forming process.

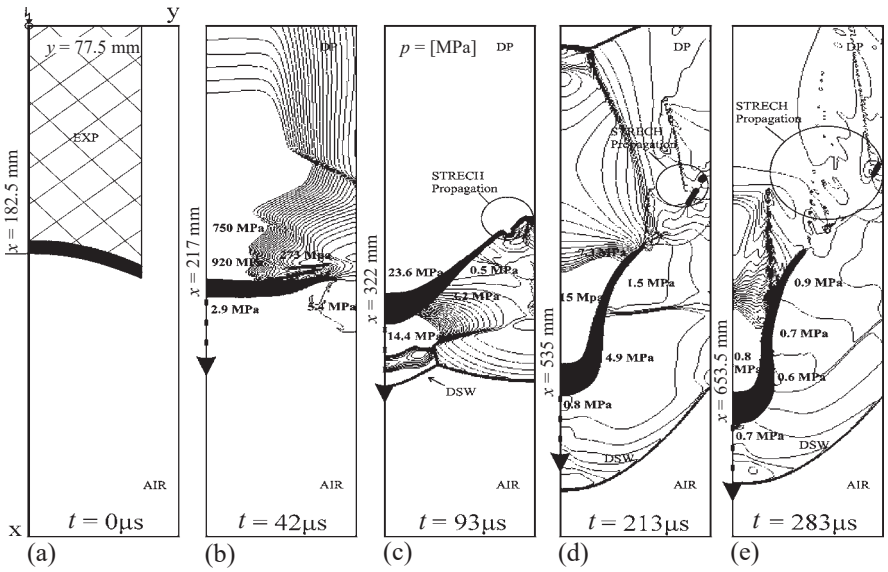

Figure 3. Simulated Projectile forming process under distributed loading of total pressures on rearward of explosion and backward of shock waves on the liners surfaces in time sequences

Front and back pressures are the projectile's external loadings. Characteristic causes and consequences of pressure loadings are appearing the detached shock waves, disposed out of front liner's layer (DSW, fig. 3).

This causes high overpressures of the DSW during, detaching of liners top fig. 3(c) and fig. 3(d), as well as, later decreasing in DSW approach phase to the top of front liners layer, fig. 3e. The edges and central parts of the liner are exposed to the of high pressure differences, which attack back layer (fig. 3). Force made by pressure differences causes velocity differences and stretch of the less thick, edging elements, which provoke liner's mass loss fig. 3. As the main cause of the drag force during motion is the DSW simulated in [1, 2], Figure 4 represents evolution of the temperatures from the DP at the end of explosive charge consumed, after 21 μs of initiation, and at the very beginning of the explosively driven propulsion of the liner. The detonation temperature is 4010 K, [27], and velocity of projectile is zero before about 21-25 μs, but they rapidly increase after liner starts to move and plastically deforms during transformation.

After rapid ejection of plastic deformable liner, the front surface, which propagates through the environmental air by the generated velocity also make the temperatures' changes of DSW, fig. 3. DSW runs of the liner's front according to adopting of blunt body effect on the accelerated velocities fig. 3(c). Temperature increased according to the DSW dispose forward of the EFP blunt body shape fig. 3(b). Plastic deformation of EFP, fig. 3(b) and fig. 3(c) change front liner's curve and diminishing blunt body effect. Converged velocities of liner's elements causes rapid decreasing of front, DSW distance causing air temperatures decrease in the stagnation zones on the front of the final formed EFP, fig. 3(d), effect.

This causes rapid decrease of front air temperature according to the achieved velocities of the final form of EFP, fig. 3(d). Final velocity of the projectiles is the 283 μs and appropriated pressures on the fig. 3, corresponds to the temperatures values of about 900 K on the top of the detached shock, as well as, very high temperature values in the stagnation zone between DSW and front layer of about 2000 K [28]. It is also important to note for the data given on the

fig. 4 that liner's tailed stretching zones have the highest temperatures of the liner's elements and mass losses were expected in simulation.

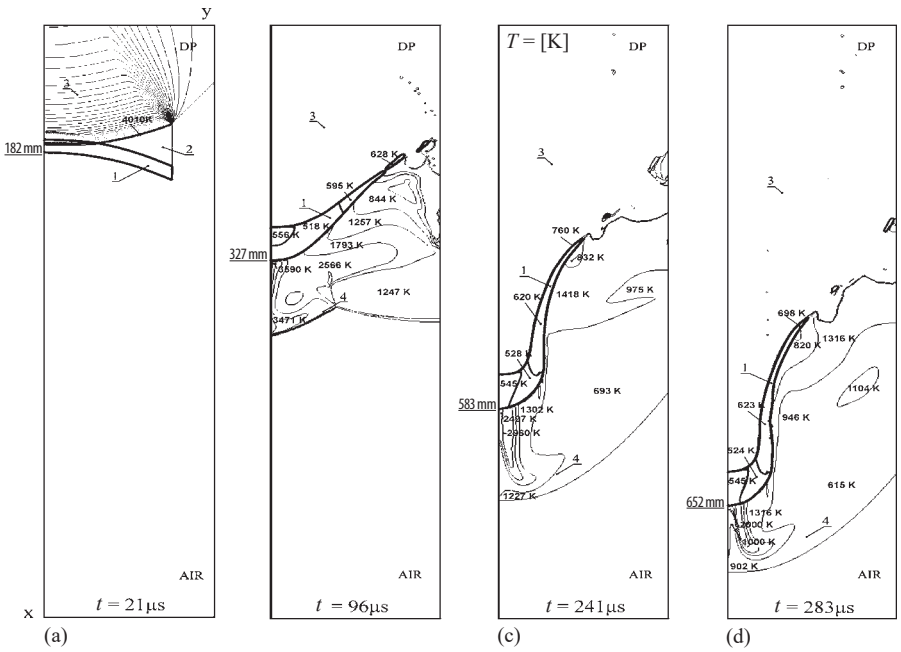

Figure 4. Simulated projectile formation and temperatures' distribution of process in time sequences on the observed; 1– liner, 2 – explosive, 3 – DP, and 4 – DSW

Sequences analyses of the liner's particular points behavior

The appropriate numeration of the segments of the particular liner's elementary volumes and brief simulations obtained three characteristic time sequences of forming processes (fig. 5) and separated parts of liners masses.

It is visible from the characteristic time sequences that plastic deformations are influenced on the layers thicknesses distribution during process and, consequently, on the further testing data caused by axial and radial displacements of dynamical points signed by numbers at the initial liners position. Elementary volumes are the rings, designed by rotational cross-section of the segments' thicknesses, at the corresponding point, and have uniform values of parameters, obtained from simulation in these points. Effective plastic strain (EFF. PL.STN on the figs. 6 and 8) behavior *vs*. full processing time is presented for each elementary volume of the liner's front layer, on fig. 6(a), and for the back layer on fig. 6(b). This liner's points approach shows non-uniform effects of plastic deformations for the elementary volumes of the back and front copper liners' layers.

It is the consequence of the different pressure conditions of the front and back elementary contact layers, precisely determined by the pressure field given as the simulation data, from fig. 3.

Stretched volumes and mass loses in the particular points are visible on fig. 5 (element No. 30). Also, these effect is indicated by the dropped or descending curves on the figs. 6-9 at the appropriated instates, where, also, other elements, as it 15 and 29, are stretched but

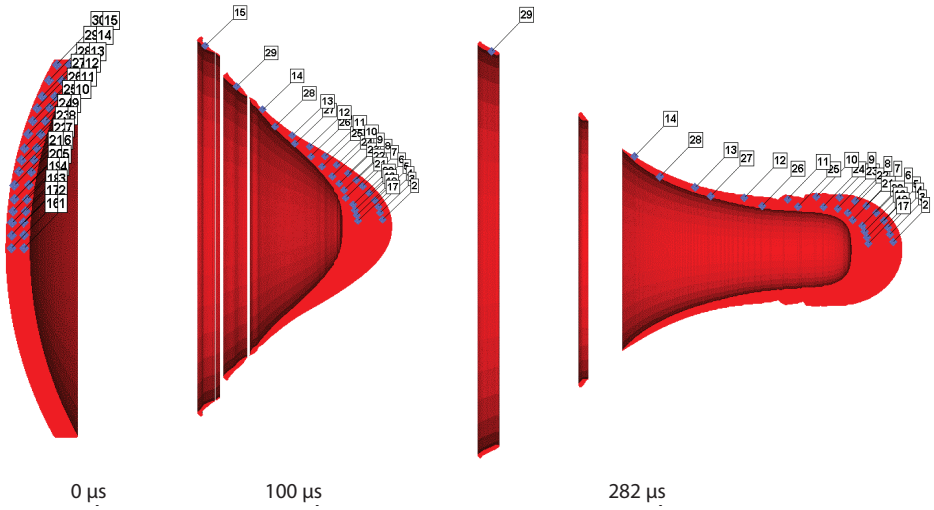

Figure 5. Obtained simulaton results of the projectile formation and mass streching in the gauge points *vs.* time (*for color image see journal web site*)

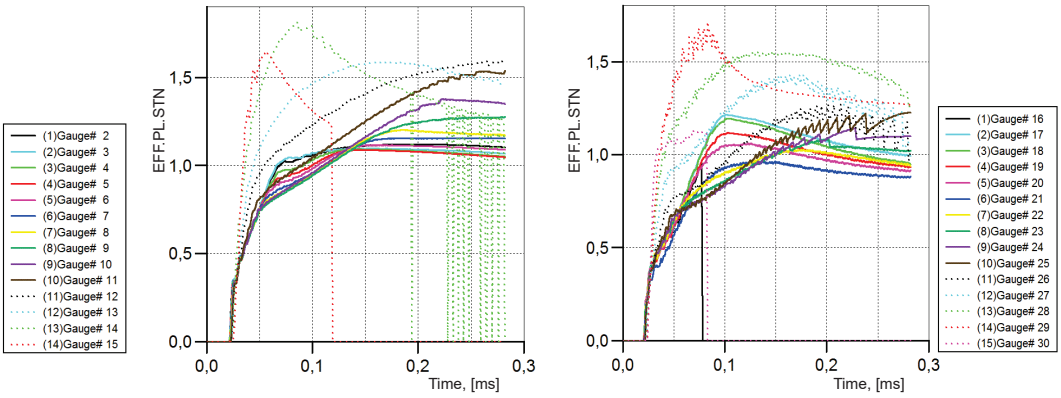

(a) The front layer (pointing in the direction of motion) of liner (b) The back layer (in contact with the explosive) of liner

Figure 6. Effective plastic strain *vs.* time of elementary volumes in gauging points during explosively forming process (*for color image see journal web site*)

remained in the control area, and continue to be treated numerically. Generated temperatures profiles along liners layers are shown on figs. 7(a) and 7(b). For each elementary volume, the temperatures are less than 760 K and much less than the copper melting point of about 1100 K. The liner's temperatures increased with two observed gradients one higher and the other lower. Higher gradients for the front, fig. 7(a), and for the back layers fig. 7(b) increased rapidly and temperature achieved 400 K for the front, and 450 K for the back layers within few μs. In the sequence "A", fig. 8, both liners' sides increased temperatures under the shock of detonation wave.

After about 100 μs, temperature gradients changes, from higher to the lower values when velocity gradients, change the sign, fig. 9, achieving temperatures of about 500 K for the

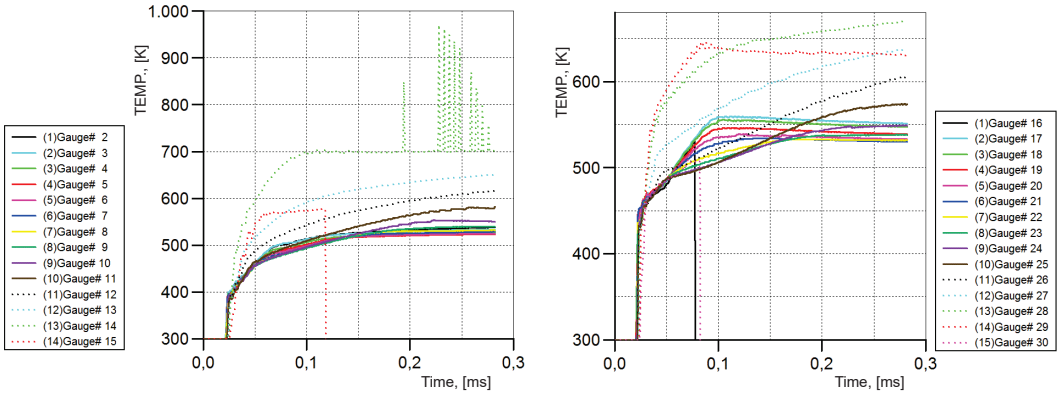

(a) The front layer (pointing in the direction of motion) of liner

(b) The back layer (in contact with the explosive) of liner

Figure 7. Consequence temperatures of elementary liner's volumes deformation *vs.* time in gauging points during explosively forming process (*for color image see journal web site*)

front layer, to 600 K for the back layer. The same effect is visible on the graph of average temperatures vs. testing time, for the variable materials exposed in the paper [17].

The most of back layer points achieved approximately the same temperature of about 530-550 K, as well as front leyer points that slowly increase to the similar values. This differences are the consequences of velocity differences in the particular points appears higher on the front than on the back liner's layers shown on figs. 7(a), 7(b), 9(a), and 9(b). In addition, it is visible that front layer and back layer points, close to edges of liner, have the highest achieved temperatures for the points 12-15, as well as, 27-30, figs. 7(a) and 7(b). Simulation model recognizes separated mass points during sequences, and is stopped, if point is ejecting out of control surface as well as if unsteady state temperatures' oscillations appears. Result is descent curve to the zero values, after separated mass particles have been ejected from the control volume. The most important conclusion from the graphs, figs. 8(a) and 8(b), is that the relation between temperature and effective plastic strain, for the both, liner's layers, front and back layers, has linear relationships. This is in accordance with authors [1, 2], which stated this behavior as the main condition for the proper forming of EFP. Relations between temperatures *vs*. effective plastic strains in both sequences keep constant temperature gradients along all liner's points, front and back layers dispersed around the central line, but different in sequences "A" and "B". Front layer point's gradients, in sequences "A" and "B" are the same and equal with back layer liner's points for the corresponding sequences. These values for the sequence "A" are about $dT/d\varepsilon_A = 464 \pm 54$ [100 K%$^{-1}$] and for the sequence "B" about $dT/d\varepsilon_B = 148 \pm 18$ [100 K%$^{-1}$]. The differences of temperature gradients appeared by the displacements of layer's points are with errors about 11-12%. Explosive propulsion, which formed bigger displacements of the layer points along axes and mixed front and back layers points cannot, provide the same temperature gradients vs. effective plastic strain of layers in all sequences of projectile generation.

Strain errors of about 11-12% corresponds to the mass loses of same process and after 125 μs which also could be the cause of different temperature gradients. Velocities' components, along *x* axes, of liner's front and back layers point's *vs*. time are shown figs. 9(a) and 9(b). The observed curves of the *x* velocity's components as the profiles *vs*. time of the front layer, fig. 9(a), and the back layer, fig. 9(b), layers' points, converge in to the final absolute velocity of about 1569 m/s orientated in the x-direction after 283 μs. Radial components of velocities

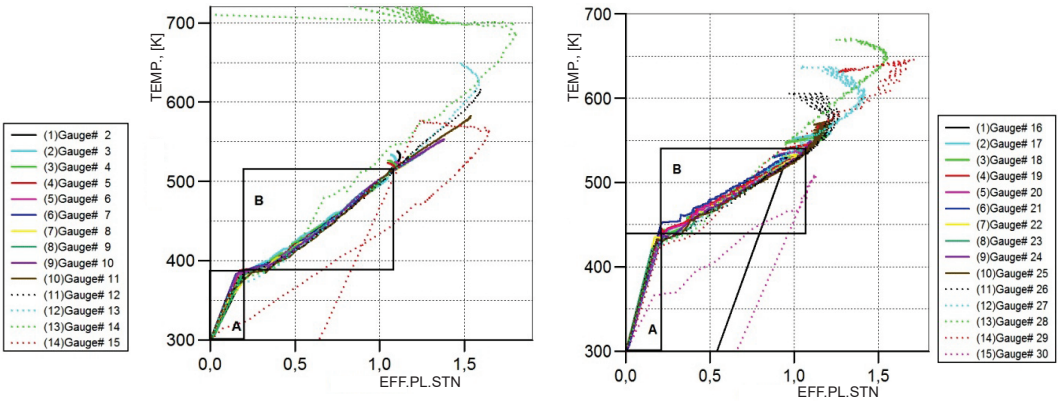

(a) The front layer (pointing in the direction of motion) of liner (b) The back layer (in contact with the explosive) of liner

Figure 8. Temperature effective plastic strain corelations of dynamical effects in the gauging points of the explosively forming process (*for color image see journal web site*)

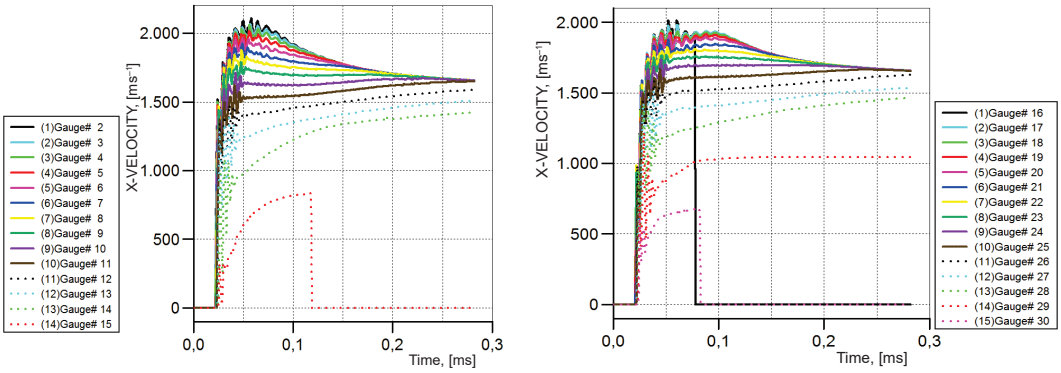

(a) The front layer (pointing in the direction of motion) of liner (b) The back layer (in contact with the explosive) of liner

Figure 9. Longitudinal velocities distributed along x-direction *vs.* process time
(*for color image see journal web site*)

orientated in the y-direction, which converge to zero values for the both layers, shown on figs. 10(a) and 10(b), and proved that explosively driven forming process is ended and radial displacements of elementary volumes have finished, also after 283 μs. These velocities' distributions are responsible for the final forming time and for the appropriate final quality of projectile shaping during explosively driven propulsion.

Finally, positive remarks, are that, papers [1] (part 1, p. 285), and [2] (p. 167), as well as paper [17], obtained similar values for the liners' temperatures as in this research. Relations of temperatures *vs*. effective plastic strains exposed in the paper [16], also proved data obtained in this papaer. Velocities distributions, simulated in this paper, shows well screening with data obtained in the paper [14].

Final discusion and conclusions

During shaping EFP had aproximatelly uniform temperature distribution along body thickness based on the conclusion that strains stop to change significantly *vs*. flight. Final velocity obtained by numerical simulation happens at the instant 283 μs, with average absolute

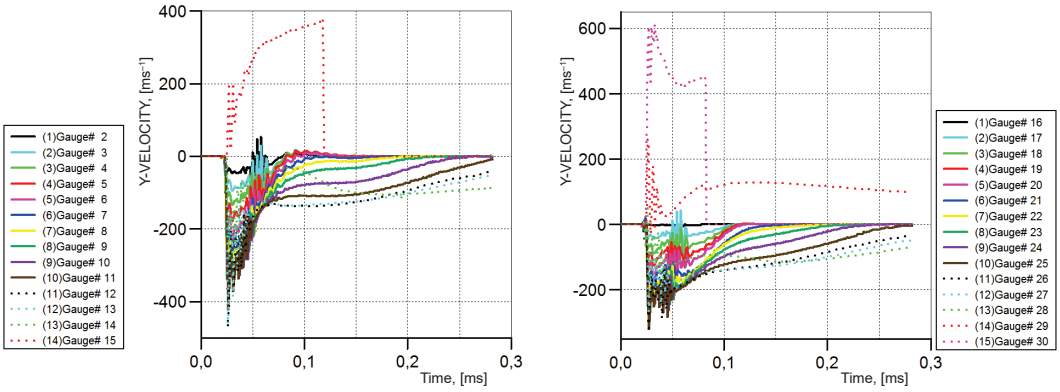

(a) The front layer (pointing in the direction of motion) of liner

(b) The back layer (in contact with the explosive) of liner

Figure 10. Radial velocities distributed along y-directions *vs.* process time
(*for color image see journal web site*)

velocity about 1569 m/s at the distance of about 471 mm, and is uniformly along surface layers. Delaying velocity effects between liners' parts makes conditions for the possible increase of the tensile effective strain. Numerical model is proved as the tool for design in analysis of projectile shape and its dynamical behavior, and expose well screening with data about liners temperatures given in the mentioned papers. Obtained relations of temperatures *vs*. effective plastic strains are shoewn well data screening. Further researches have to consider the effects of different liner's materials, explosive charges with, different explosive materials, as well as different initial forms of liners and charges. These variations can give more data about reasons for the invariant temperatures gradients *vs*. effective plastic strains along liners thickness during two main sequences of the processes. In addition, this has to orientate the new approach of performances and the main influences, analyses important for the required new missions of EFP as the part of missiles' payloads.

Acknowledgement

The Ministry of Education, Science and Technological Development of the Republic of Serbia, through the project III-47029, support this research in 2015, which is gratefully acknowledged.

Nomenclature

A – chosen coefficient, [–]
A_1 – semi-empirical coefficient, [–]
B – chosen coefficient, [–]
B_1 – semi-empirical coefficient, [–]
C – chosen coefficient for, [–]
c_p – specific heat, [kJkg^{-1}K^{-1}]
D – detonation velocity, [ms^{-1}]
E – detonation energy, [kJm^{-3}]
k_i – co-volume factor, [–]
m – thermal softening exponent, [–]
n – hardening exponent, [–]
P – pressure in Chapman-Jouget, [kPa]
p – pressure of detonation products, [Pa]
R – universal gas constant, 8.315, [Jmol^{-1}K^{-1}]
R_1 – semi-empirical coefficient, [–]
R_2 – semi-empirical coefficient, [–]
T – current temperature, [K]
T_H^* – homologous temperature, [K]
T_M – melting temperature, [K]
T_R – room temperature, [K]
T_0 – initial temperature, [K]
t – time, [μs]
V – reduced volume, v/v_0, [–]
v – current specific volume, [m^3 kg^{-1}]
v_g – molar volume of gas, [m^3 mol^{-1}]
v_0 – initial specific volume, [m^3 kg^{-1}]
x_i – mole fraction, [–]

Greek symbols

α – fitting coefficient, [–]
β – fitting coefficient, [–]
γ – heat capacity ratio, [–]
ε – effective plastic strain EFF.PL.STN, [–]
$\dot{\varepsilon}$ – effective plastic strain rate, [s^{-1}]
θ – fitting coefficient, [–]
ρ – current density, [kgm^{-3}]
ρ_{air} – air density, [kg m^{-3}]
ρ_0 – initial density, [kgm^{-3}]
χ – fitting coefficient, [–]
ω – semi-empirical coefficient, [–]

Subscripts

g – gas, [–]
i – i-th products, [–]
M – melting, [–]
R – room

Acronyms

BKW – Becker Kistiakosky Wilson
DP – detonation pressure
DSW – detached shock waves
EFP – explosively formed projectile
EOS – equation of state
JWL – Jones Wilkins Lee

References

[1] Orlenko, L. P., *Fizika Vzryiva (part 1, 2),* (Physics of Explosion – in Russian), Glavnaya redaktsiya fizichesko matematicheskoy literaturi, Moscow, Russia, 2004
[2] Bender, D., Corleone, J., *Tactical Missile Warheads*, American Institute of Aeronautic and Astronautic, Washington DC, USA, 1993
[3] Lloyd, M. R., *Conventional Warhead Systems Physics and Engineering Design*, American Institute of Aeronautic and Astronautic, Restona, Va., USA, 1998
[4] Jaramaz, S., *Warhead Design and Terminal Ballistics,* Faculty of Mechanical Engineering, Belgrade, 2000
[5] Bender, D., *et al*., Explosively Formed Penetrators (EFP) with Canted Fins, *Proceedings*, 19th International Symposium of Ballistics, Interlaken, Switzerland, 2001, pp. 755-762
[6] Marković, D. M., Explosively Formed Projectiles, M. Sc. thesis, University in Belgrade, Belgrade, 2011
[7] Alekseevich, V. O., Guided Missile in Beam Warhead, Russian Federal Service for Intellectual Property, Patents and Trademarks, 2007120497/02, 2007
[8] Comstock, M., *et al*., Combined Effect Explosively Formed Penetrator Warhead Development, U. S. Army RDECOM-ARDEC, *Proceedings*, The 24th Army Science Conference, Orlando, Fla., USA, 2005, pp.1-3
[9] Jaramaz, S., Micković, D., Military Applications of Explosive Propulsion*, FME Transaction*, *30* (2002), 1, pp. 15-22
[10] Jaramaz, S., *Physics of Explosion*, Faculty of Mechanical Engineering, Belgrade, 1997
[11] Regueiro, R. A., Horstemeyer, M. F., CTH Analysis of Tantalum EFP Formation Using the BCJ Model: CA 94551-0969, Center for Materials and Engineering Sciences, Sandia National Laboratories, Livermore, Cal., USA
[12] Marković, M., *et al*., Numerical and Analytical Approach to the Modeling of Explosively Formed Projectiles, *Proceedings*, 6th International Scientific Conference – OTEH 2014, Belgrade, 2014, pp. 9-10
[13] Marković, M., *et al*., Numerical Modeling of Temperature Field on High Velocity Explosively Formed Projectile, *Proceedings*, 17th Symposium on Thermal Science and Engineering of Serbia, Sokobanja, Serbia, 2015, pp. 175-181
[14] William, J. F., Analytical Models of the Projection Angle of Explosive Accelerated Liners, *Proceedings*, 15th International Symposium on Ballistics, Jerusalem, Israel, 1995, pp. 243-251
[15] Lam, C., McQueen, D., *Study of the Penetration of Water by an Explosively Formed Projectile*, DSTO-TR-0686, Aeronautical and Maritime Research Laboratory, Melbourne, Australia, 1998
[16] Pappu, S, Murr, L. E., Hydrocode and Microstructural Analysis of Explosively Formed Penetrators, *Journal of Materials Science*, *37* (2002), 2, pp. 233-248
[17] Hussein, G., *et al*., Analytical Performance Study of Explosively Formed Projectile, *Journal of Applied Mechanics and Technical Physics*, *54* (2013), 1, pp.10-20
[18] Fedorov, S. V., *et al*., Numerical Analysis of the Effect of the Geometric Parameters of a Combined Shaped-Charge Liner on the Mass and Velocity of Explosively Formed Compact Elements, *Combustion, Explosion, and Shock Wave*, *51* (2015), 1, pp. 130-142
[19] Jianfeng, L., *et al*., Numerical Simulation of Formation of EFP with Charge of Aluminized High Explosive, *Proceedings*, International Symposium on Ballistics, Tarragona, Spain, 2007, Vol. 1, pp. 1265-1271

[20] Johnson, G. R., Stryk, R. A., Some Considerations for 3D EFP Computations, *International Journal of Impact Engineering, 32* (2006), 10, pp. 1621-1634
[21] ***, AUTODYN User manual version 14.0
[22] Luttwak, G., Cowler, M. S., Advanced Eulerian Techniques for the Numerical Simulation of Impact and Penetration using AUTODYN-3D, *Proceedings*, International Symposium of Interaction of the Effects of Munitions with structures, Berlin, Germany, 1999, Vol. 9, pp. 441-449
[23] Hussein, G., *et al*., Gradient Valued Profiles and L/D Ratio of Al EFP With Modified Johnson Cook Model, *Journal of Materials Science and Engineering*, *5* (2011), May, pp. 599-604
[24] Teng, T. L., *et al*., Design and Implementation of a High Velocity Projectile Generator, *Combustion, Explosion, and Shock Waves*, *43* (2007), 2, pp. 233-240
[25] Fong, R., *et al.,* 3D Hydro Code Analysis of Novel Asymmetrical Warhead Designs, *Proceedings*, The 24th Army Science Conference, Orlando, Fla., USA, 2005, pp.1-3
[26] Jing, P. L., *Evaluation of the Thermochemical Code-CHEETAH 2.0 for Modeling Explosives Performance*, DSTO-TR-1199, Aeronautical and Maritime Research Laboratory, Melbourne, Australia, 2001
[27] Keshavarz, M. H., Correlations for Predicting Detonation Temperature of Pure and Mixed CNO and CHNO Explosives, *Indian Journal of Engineering and Materials Sciences*, *12* (2005), 2, pp.158-164
[28] Anderson, J. D., *Hypersonic and High Temperature Gas Dynamics*, American Institute of Aeronautics and Astronautics, Restona, Va., USA, 2006

Paper submitted: December 17, 2015
Paper revised: March 14, 2016
Paper accepted: April 3, 2016